Journal of Current Research in Oral Surgery
2025, Volume 5, Issue 2, Page No: 100-112

Available online at: www.tsdp.net

ISSN: 3062-3480

Original Article

Deep Learning–Based Diagnosis of Elongated Styloid Process: A Comparative Study of EfficientNetB5 and InceptionV3

Chen Hao[1]*, Liu Fang[1], Zhao Lin[2]

[1]Department of Oral and Maxillofacial Surgery, Faculty of Stomatology, Zhejiang University, Hangzhou, China.
[2]Department of Surgical Dental Sciences, Faculty of Medicine, Nanjing University, Nanjing, China.

***E-mail** ✉ chen.hao@outlook.com

Received: 19 April 2025; **Revised:** 23 August 2025; **Accepted:** 27 August 2025

ABSTRACT

A bony projection arising from the temporal bone, termed the styloid process (SP), can undergo excessive lengthening and give rise to neck pain, throat irritation, and cephalalgia. This overgrowth, linked to Eagle syndrome, may exert pressure on adjacent nerves and vessels, occasionally triggering serious sequelae. The conventional imaging-driven categorization of elongated styloid process (ESP) variants is hampered by inconsistent radiographic quality, varying patient positioning, and individual anatomical variation—factors that, together, constrain diagnostic confidence. Modern strides in artificial intelligence, especially within deep learning, now permit a more robust classification workflow for ESP. The present work set out to engineer an automated ESP classification pipeline powered by deep learning models and to systematically compare the classification capabilities of two distinct network designs, EfficientNetB5 and InceptionV3. A retrospective design was adopted, with Orthopantomograms (OPGs) from our institutional oral radiology database used to classify ESP. The ImageJ application was used to measure the lengths of styloid processes. A curated collection of 330 elongated and 120 normal styloid process images formed the basis for model training and testing. Image preparation incorporated median filtering and dimensional resizing, and augmentation techniques were applied to strengthen generalisability. Both EfficientNetB5 and InceptionV3 served as feature-extraction backbones, each learning distinctive styloid-process representations. Model outputs were benchmarked on accuracy, precision, recall, and F1-score, and the resultant figures were compared side by side to determine which architecture offered greater clinical promise. The EfficientNetB5 model achieved 97.49% accuracy, 98.00% precision, 97.00% recall, and 97.00% F1-score, indicating a high level of discriminative power. Its AUC reached 0.9825. The InceptionV3 model achieved 84.11% accuracy, 85.00% precision, 84.00% recall, and an F1-score of 84.00%, with an AUC of 0.8943. Across all evaluated performance dimensions, EfficientNetB5 consistently exceeded InceptionV3. To summarise, this investigation delivers a deep learning–based solution, built on EfficientNetB5 and InceptionV3, for assigning elongated styloid processes to distinct morphological categories using digital panoramic radiographs. The evidence gathered suggests that these tools—above all, EfficientNetB5—can improve diagnostic accuracy and streamline clinical workflows, ultimately aiding the delivery of higher-quality patient care.

Keywords: Deep learning, Panoramic radiography, Convolutional neural networks, Styloid process, Diagnosis

How to Cite This Article: Hao C, Fang L, Lin Z. Deep Learning–Based Diagnosis of Elongated Styloid Process: A Comparative Study of EfficientNetB5 and InceptionV3. J Curr Res Oral Surg. 2025;5(2):100-12. https://doi.org/10.51847/qwDKS23PRX

Introduction

The styloid process (SP) is an elongated cylindrical osseous spur descending from the lower border of the petrous temporal bone and occupying a lateral cervical position sandwiched by the carotid arterial system and the internal jugular vein. It fulfills a critical biomechanical role in oropharyngeal motion. Embryologically, the structure derives from cartilage

of the second pharyngeal arch; bone deposition begins in the third prenatal trimester and continues into the first decade of postnatal life. Multiple muscles and ligamentous bands attach to it, heavily influencing oropharyngeal kinetics. Reports place the prevalence of an elongated styloid process anywhere from 3.3% to 84.4% [1].

The condition, now known as Eagle syndrome, is characterized by the co-occurrence of an elongated styloid process (ESP) and orofacial discomfort. The hallmark consists of pharyngeal pain radiating to assorted cervicofacial zones [2].

The clinical picture accompanying elongation covers a wide spectrum: cervical ache, pharyngeal irritation, otalgia, globus sensation, position-dependent head and neck pain, odynophagia, shoulder soreness, and a choking feeling. The elongated styloid process (ESP) can provoke these complaints via multiple pathological routes—irritation of the glossopharyngeal, vagal, or trigeminal nerve branches; impingement on carotid vessels sufficient to induce carotidynia or carotid artery syndrome; degenerative or inflammatory processes at the tendinous stylohyoid insertion (insertion tendinitis, also called hyoid syndrome); and post-infectious rheumatic styloiditis originating from pharyngeal inflammation. Severe cerebrovascular events such as transient ischemic attacks or stroke represent rarer but recognized outcomes of carotid compression [3]. The standard SP length is estimated at 20–30 mm, measured from the point of tympanic plate emergence to the tip. Any measurement exceeding 30 mm qualifies as elongated and may occur on one or both sides. Typically, an elongated styloid process surfaces incidentally during routine dental appointments and radiographic surveys. Ossified bands are included when gauging total process length. The fundamental trigger for elongation remains elusive [4]. Clinical pain has been attributed to earlier trauma fracturing the process or to prior tonsil surgical removal. Other explanations in the literature encompass congenital lengthening, partial or complete ossification of the stylohyoid chain, delayed maturation at the tympanohyale–stylohyoid cartilaginous junction leading to overgrowth, post-traumatic reactive hyperplastic changes, and a suspected connection with early menopausal transition [5].

Radiologically, meticulous evaluation of elongated styloid processes is necessary to distinguish the condition from neurological mimics, including glossopharyngeal neuralgia, persistent cephalalgia, cervical soreness, migraine, and lightheadedness. Investigators have employed a spectrum of radiographic tools to study the elongated styloid process (ESP)—among them lateral head and neck films, posteroanterior skull views, exaggerated Towne's projections, orthopantomography (OPG), lateral oblique mandibular radiographs, anteroposterior skull images, Cone Beam computed tomography, and computed tomography. CT scanning can map out the length, inclination, and spatial relationships of the styloid process. That said, orthopantomography is often the modality of choice. OPG constitutes a two-dimensional imaging method that serves as the frontline radiographic investigation for the extraoral dento-maxillofacial complex. Its widespread availability, reduced radiation burden, and cost savings compared to CT make OPGs a go-to option when surveying orofacial abnormalities. The technique is easy both to perform and to read.

What is more, elongation of the SP can be spotted on an OPG with substantial reliability [6-9]. Reliably sorting elongated styloid processes into morphological subtypes is fundamental to appropriate clinical management, encompassing both diagnostic workup and therapeutic strategy. Langlais *et al*. [10] advanced a morphology-based ESP taxonomy: Type I takes an uninterrupted form; Type II exhibits a pseudo-articulated configuration; and Type III appears segmented. Conventionally, ESP classification has leaned on manual scrutiny of digital panoramic radiographs by seasoned radiologists or clinicians. This pathway, however, is labor-heavy, slow, and open to individual interpretation, inviting inconsistencies and diagnostic misjudgments. On top of that, traditional categorization approaches may fail to capture subtle morphological differences among elongated styloid processes, which are significant for treatment choices and patient trajectories.

Artificial intelligence (AI) is reshaping dental radiology, with its chief applications including image analysis and reading, treatment blueprinting, patient communication, and scientific inquiry. AI algorithms demonstrate proficiency in parsing dental radiographs to flag pathological changes, and, via deep learning, they tease out patterns and image signatures, equipping dentists with findings that are both more precise and delivered more rapidly. The upshot is improved patient care and superior therapeutic endpoints. Quality control is indispensable in dental radiology, and AI plays a role in safeguarding the fidelity and trustworthiness of radiographic images. By identifying defects such as artifacts and suboptimal exposure, AI-driven tools improve the overall quality of radiographic exams, boosting diagnostic certainty [11]. A body of work has fruitfully applied AI algorithms to the measurement of morphometric parameters of the cranium, including maxillary and mandibular landmarks. These tools provide precise figures with

high reliability and accuracy, helping distinguish normal anatomy from deviations. Over recent years, enthusiasm has grown for deploying advanced computational frameworks—chief among them deep learning—to mechanize the sorting of medical imaging data. Deep learning architectures, exemplified by convolutional neural networks (CNNs), have demonstrated striking skill at distilling informative features from imagery and reliably ordering complex patterns [12-14]. Image sorting and feature extraction proceed with great fidelity, converting raw input into actionable output that may take the shape of "image categories," "object locations," and "pixel labels." Such deep learning classifiers stack numerous convolutional layers before fully connected layers, achieving object recognition levels that equal or exceed those of human operators. By leveraging deep learning's capabilities, one can develop ESP classification systems that are both more performant and more reliable. The study at hand set out to deploy deep learning models and measure the classification and diagnostic performance of two designs—EfficientNetB5 and InceptionV3—when applied to elongated styloid processes.

Materials and Methods

Older approaches to pinpointing and typing the elongated styloid process have proven challenging because they must contend with the inherent fluctuations in digital panoramic radiographs—driven by uneven image quality, differences in patient positioning, and inherent anatomical variation from one person to the next. Such limited adaptability can undermine their accuracy when called upon to classify elongated styloid processes across a diverse patient population. In addition, older methods may struggle to capture the complex relational cues in images of elongated styloid processes. As a consequence, picking up on the faint patterns or distinctions that are pivotal for correct categorization may not be feasible, yielding substandard results.

In the current work, the approach for distinguishing among the different elongated styloid process types begins by assembling real-world digital panoramic radiographs from clinical storehouses (the archival holdings of our oral radiology unit). These images serve as the substrate for our deep learning models, which are built and tested on them. The study was designed to conform to the ethical principles of the Helsinki Declaration and obtained Institutional Review Board approval. Every procedural step was carried out in accordance with the pertinent guidelines and statutory requirements attached to the ethics approval. Owing to the study's retrospective character, the Institutional Review Board Committee of SRM Dental College waived the requirement for informed consent.

A sum of 931 orthopantomograms (OPG) formed the study corpus. Each radiograph belonged to male or female subjects who had presented to the dental outpatient clinic for standard oral health screening and evaluation. Digital images meeting a satisfactory resolution threshold were retained. By contrast, images of individuals under 18 years of age, duplicate files, and those marred by distortion or artifacts were discarded. Images where superimposition by adjacent structures left the styloid processes poorly visible were ruled out. Radiographs displaying substandard patient alignment, insufficient resolution, and those tied to subjects with maxillary or mandibular surgical defects or trauma were likewise removed from the working set. In this manner, the starting tally of 938 was reduced to 330 OPG images. A single standardized observer selected orthopantomograms (OPGs) suitable for styloid process measurement, in accordance with the predetermined inclusion and exclusion criteria. With the aid of ImageJ software (National Institute of Health, Maryland, USA), the observer gauged each styloid process's length, defined as the linear span from its takeoff point on the temporal bone to its terminal tip. To curtail potential bias or examiner fatigue-induced errors, no more than 20 radiographs were scrutinized per day.

Thereafter, a compilation was assembled encompassing 330 images—capturing unilateral and bilateral cases demonstrating elongated styloid processes —alongside 120 images representative of styloid processes within the standard length range. Partitioning of this compilation into instructional and evaluative subsets was carried out thus: one-fifth of the radiographic material (90 images in total) was held back as a dedicated "test set." Adopting this split meant the evaluation batch would consist solely of radiographic views the model had never processed during its learning cycle. The outstanding 360 radiographs were funneled into the training and validation segments. Any styloid process whose linear dimension, traced from the tympanic plate exit site to its distal apex, stayed within the 20–30 mm bracket was labeled "Normal"; those recording lengths beyond the 30 mm threshold were designated "Abnormal." Beyond this binary grouping, the assembled image repository was tagged following the taxonomic framework of Langlais *et al*. [10] under the headings: "Normal," "Pseudo Articulated," "Segmented," and "Uninterrupted," after which the images were further stratified into clusters representing bilateral elongation, elongation confined to the left side, and elongation

restricted to the right side. A Type I SP was characterized by a smooth, continuous outline across its full span; a Type II SP displayed a junction with the hyoid bone, giving rise to what is termed a "pseudo articulation"; and a Type III SP was marked by multiple interruptions or segmentations distributed along its trajectory while still maintaining a cumulative length exceeding 30 mm. Before any model instruction could begin, an indispensable preparatory intervention was undertaken to boost image refinement and discard non-pertinent visual information. This intervention relied on median filtering to dampen image noise, supplemented by rescaling the entire image dataset to a fixed-dimensional standard, to ensure uniformity across the full dataset.

After this preparatory treatment had concluded, the instructional segment of the workflow commenced. At this juncture, deliberate variation was introduced into the image pool through a suite of augmentation maneuvers; the purpose of this artificial diversification was to equip the model with a more generalizable understanding, better able to contend with data it had not previously been exposed to **(Figure 1)**. Hyperparameter refinement was then performed to optimize the model's operational settings and achieve peak performance. Throughout the training interval, batches of images were routed to a pair of deep learning frameworks, EfficientNetB5 and InceptionV3, each serving as a feature distillation module. These modules sift through raw pixel input and isolate the high-level visual signatures that distinguish elongated styloid processes from normal anatomy.

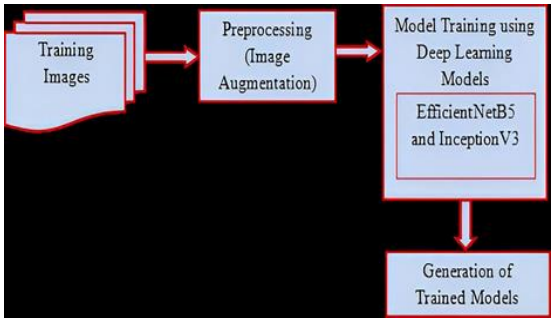

Figure 1. Training process.

Once both frameworks had completed their training cycles, the inferential stage of operations was activated. Any newly introduced image specimen was first subjected to the same preparatory steps used during training, ensuring procedural consistency. After passing through this standardized preparatory pipeline, the images were fed forward into the now-trained EfficientNetB5 and InceptionV3 engines, where the built-in softmax classification layers drew upon the previously internalized feature representations to sort each image into its corresponding elongated styloid process variant **(Figure 2)**.

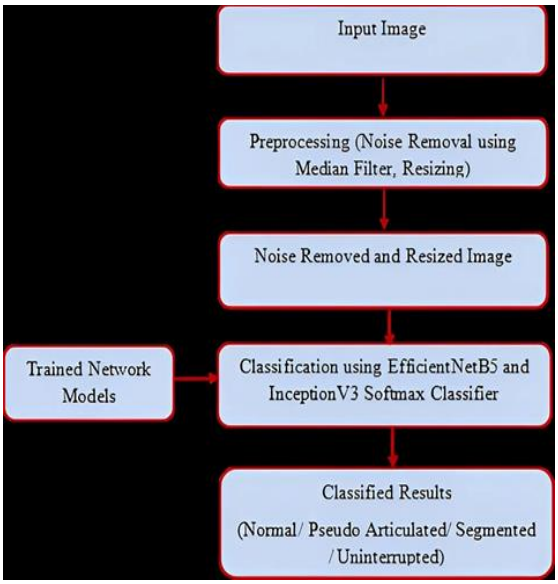

Figure 2. Testing process.

Finally, the categorical outputs from the two frameworks were subjected to rigorous comparative scrutiny, using a panel of quantitative benchmarks encompassing accuracy, precision, recall, and F1 score. A head-to-head appraisal was conducted to assess the relative competence of each framework in distinguishing among elongated styloid process types. In sum, the overarching ambition of this procedural blueprint was to forge a resilient instrument that could offer clinical practitioners tangible support in the diagnostic assessment and therapeutic strategizing for patients with elongated styloid processes, thereby advancing the quality of patient management.

Module implementation and description

The study was structured around a succession of clearly demarcated operational modules. These modules included: (1) data collection, (2) preprocessing, (3) training phase, (4) inference phase, and (5) evaluation and analysis. The computational ecosystem was built upon delineated hardware and software foundations. Hardware resources comprised a Core i5 Processor, a 500 GB Hard Disk, a 15″ LED Monitor, standard Input Devices (Keyboard, Mouse), and 4 GB of RAM. The software backbone incorporated Windows 10 and Python, executed in a Jupyter Notebook environment.

Data collection

Authentic, practice-derived digital panoramic radiographs were obtained from clinical settings, serving as the primary substrate for training and subsequently challenging the deep learning models.

These radiographic records document the natural anatomical spectrum of elongated styloid processes, delivering the core dataset indispensable for model cultivation. By drawing on images originating from genuine clinical workflows, we anchored the model's practical relevance and its readiness for deployment in real-world contexts. A methodical scheme was implemented to catalog the assorted morphological presentations of elongated styloid processes. The scheme involved the exhaustive assembly and close examination of 938 orthopantomograms (OPGs) extracted from clinical archives. Using the sophisticated ImageJ platform (National Institutes of Health, Maryland, USA), we measured the styloid process length for each included case. Building on these measurements, a refined image bank of 330 elongated styloid process instances—spanning unilateral and bilateral configurations—together with 120 normal styloid process controls was constituted. A deliberately chosen subset of images was annotated in alignment with the Langlais *et al*. [10] classification lexicon as "Normal," "Pseudo Articulated," "Segmented," or "Uninterrupted." These annotated images were next organized into partitions representing bilateral elongated styloid processes, exclusively left-sided elongation, and exclusively right-sided elongation. During the image preparation stage, whenever a single radiographic plate demonstrated bilateral elongation of the styloid process, that plate was divided into two standalone images by cropping.

Preprocessing

Before model training, a vital preprocessing step was performed to improve image quality and remove non-essential details. At the heart of this operation lay a median filtering procedure that suppressed noise, producing cleaner, more legible images. Running in parallel, the full collection of images was rescaled to a predetermined dimension (Input Image Size: 128 × 128), ensuring a uniform format across all dataset entries. This preprocessing sequence was considered foundational; it prepared the image corpus for downstream analytical tasks and ensured that deep learning models would be furnished with immaculate, standardized inputs.

Training phase

The training sequence was initiated once the preprocessing phase concluded. At this point, images were directed through a series of augmentation transformations engineered to seed the dataset with deliberate variability. Such augmentation enhanced the model's ability to extrapolate beyond its training examples. It strengthened its overall robustness, while enabling fine-tuning of operational parameters, including batch sizes (32), the ADAM optimization algorithm, and a 50-epoch schedule, all calibrated for maximal yield. Throughout training, the imagery was streamed to the two designated deep learning architectures—EfficientNetB5 and InceptionV3—which served as feature-extraction conduits. These architectures distill and encode the informative content of the input, homing in on the hallmark visual traits associated with elongated styloid processes.

Inference phase

Following the culmination of training, the inference phase was brought into operation. Freshly introduced images were funneled through precisely the same preprocessing regimen that had governed the training workflow, thereby preserving procedural uniformity. Once preprocessed, the images were advanced into the previously instructed EfficientNetB5 and InceptionV3 networks. Using their integrated softmax classification heads, the networks mapped each image to one of the elongated styloid process categories, guided by the feature patterns learned during training. This phase enabled the direct application of the developed models to real-world radiographic material, effectuating the hands-free categorization of elongated styloid processes.

Proposed algorithm

EfficientNetb5

The EfficientNet family introduces a convolutional neural network blueprint and a scaling strategy in which a single compound coefficient drives uniform changes across depth, width, and resolution simultaneously. Older practices tend to adjust these three axes in isolation; in contrast, EfficientNet enforces proportional scaling through a set of fixed coefficients. This design secures a rule-governed, even scaling of width, depth, and resolution as one moves between models. The underlying intuition for compound scaling is that a larger input image calls for a deeper stack of layers to broaden the receptive field, coupled with additional channels that can capture finer, more granular patterns in that image **(Figure 3)**.

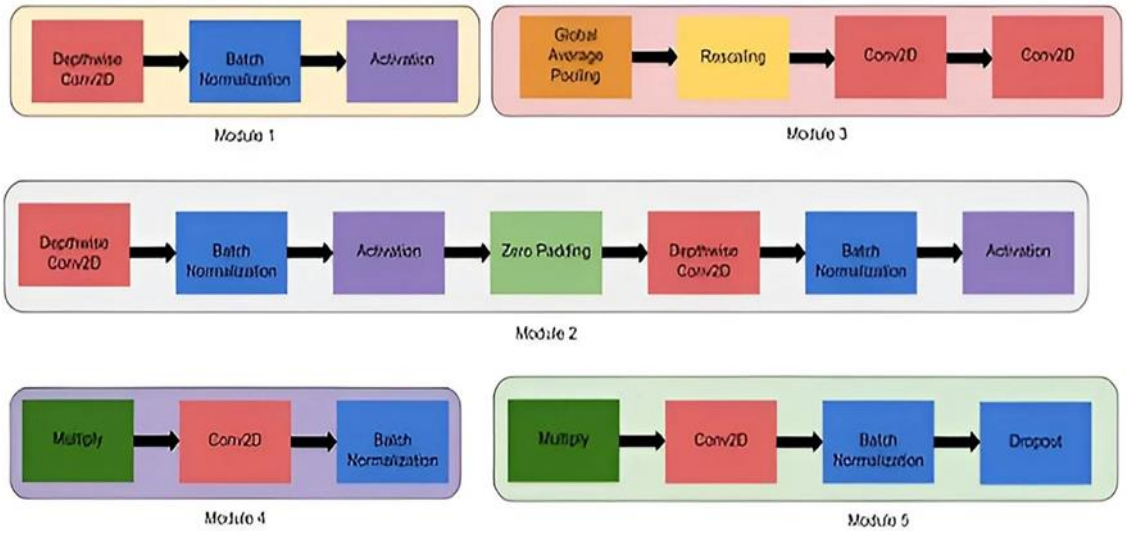

Figure 3. Architectural structure of EfficientNetB5.

Inception V3

Inception V3 is a convolutional neural network for image classification, designed as a more sophisticated successor to Inception V1 (2014). Built by Google, it incorporates a series of refinements and technical measures that improve overall performance. Compared to earlier versions, it delivers greater efficiency and keeps computational demands in check. The network remains fast despite increased layer depth and integrates auxiliary classifiers as a regularisation device. Unveiled in 2015, this 42-layer model records lower error figures. Its signature upgrades include breaking convolutions into smaller operations, spatial factorization via asymmetric convolutions, efficient grid-size shrinking, and auxiliary classifiers **(Figure 4)**.

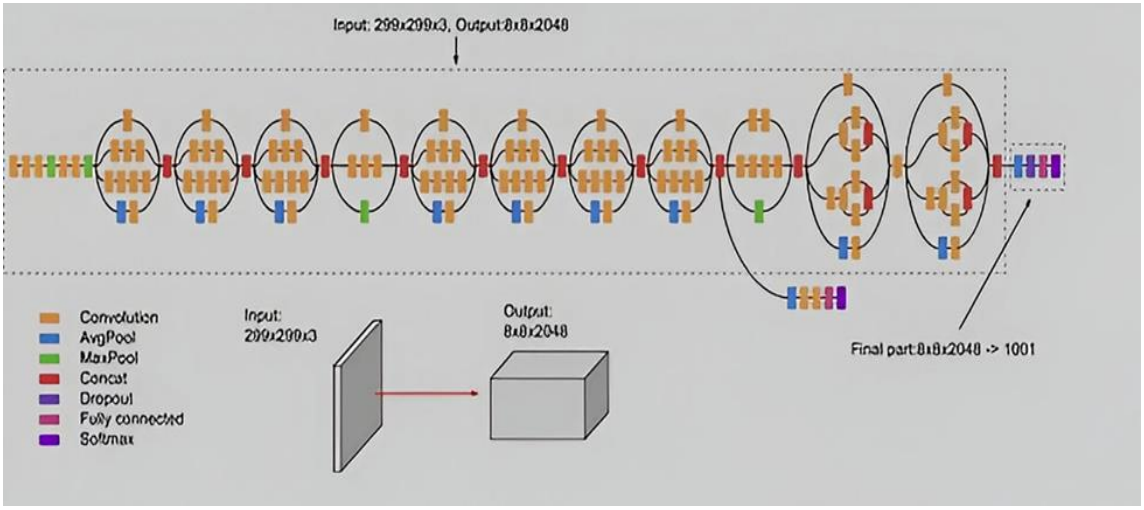

Figure 4. Architectural structure of Inception V3.

Results and Discussion

Evaluation and analysis

Classification outcomes from both models were subjected to a rigorous quantitative assessment across several performance indicators—accuracy, precision, recall, and F1 score—by aligning predicted labels with ground truth labels.

Accuracy: Quantifies the ratio of TP plus TN to the entire pool of test images.

$$\text{Accuracy} = \frac{TP+TN}{TP+TN+FP+FN} \quad (1)$$

Precision: Defined as the proportion of true positive estimations relative to the combined sum of true positive and false positive rates. An equation gives the precise formulation.

$$\text{Precision} = \frac{(TP)}{(TP + FP)} \quad (2)$$

Recall: Defined as the proportion of true positive rate estimations relative to the combined sum of the true positive and false negative rates. An equation gives the precise formulation.

$$\text{Recall} = \frac{(FP)}{(TP + FN)} \quad (3)$$

F1-Score: The F-Measure corresponds to the harmonic mean of recall and precision. In the standard F-measure (F1), the two components are weighted equally.

$$F_s(1+\varepsilon^2)\frac{\text{Recall} \times \text{Precision}}{\varepsilon^2 \cdot \text{Precision} + \text{Recall}} \quad (4)$$

Training process

Tracking the trajectory of training accuracy and loss during deep learning model training is critical for evaluating model fitness and detecting warning signs, such as overfitting or underfitting. Compared with Inception V3, EfficientNetB5 achieved higher training performance **(Figures 5 and 6)**.

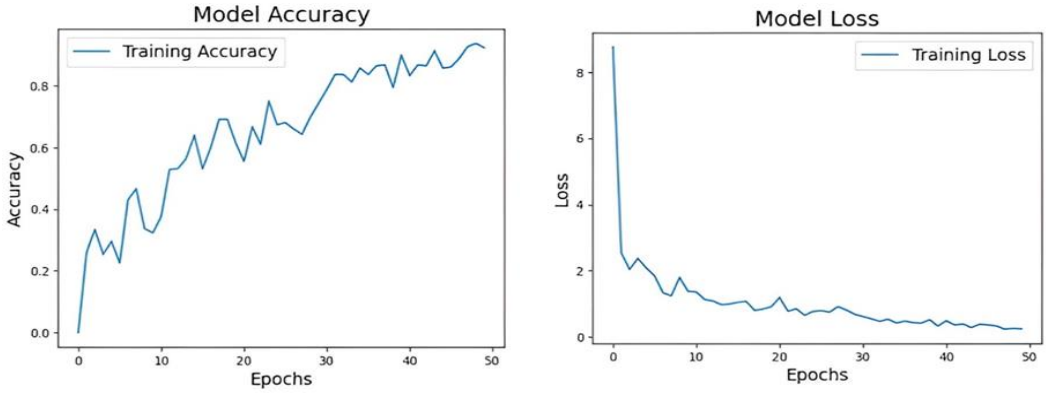


```
train_loss, train accuracy [0.11039185523986816, 0.9895833134651184]
```

Figure 5. The training accuracy and training loss of efficient NetB5.

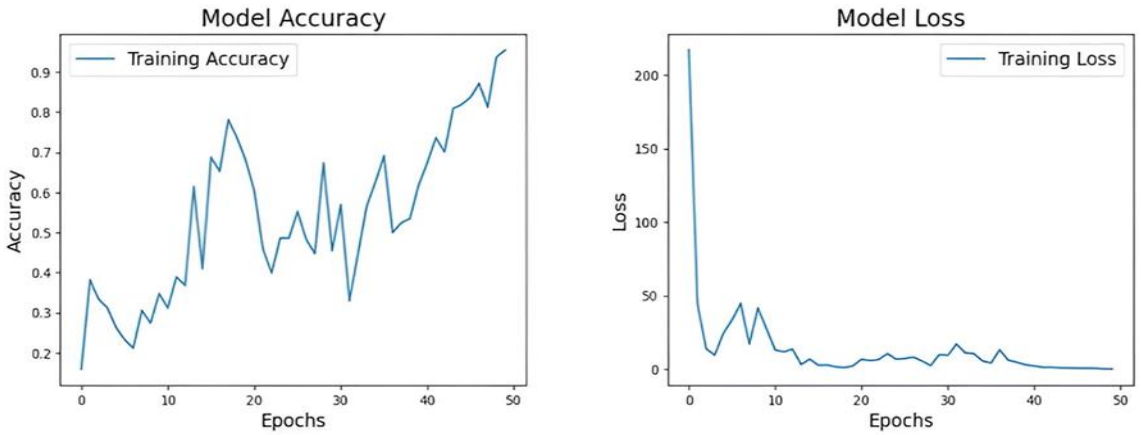


```
train_loss, train accuracy [0.13175681233406067, 0.9409722089767456]
```

Figure 6. The training accuracy and training loss of inception V3.

Testing process

The batch of preprocessed images was forwarded through the fully trained EfficientNetB5 and InceptionV3 networks, and each image was assigned to one of the elongated styloid process subtypes based on the features the models had internalized **(Figure 7)**.

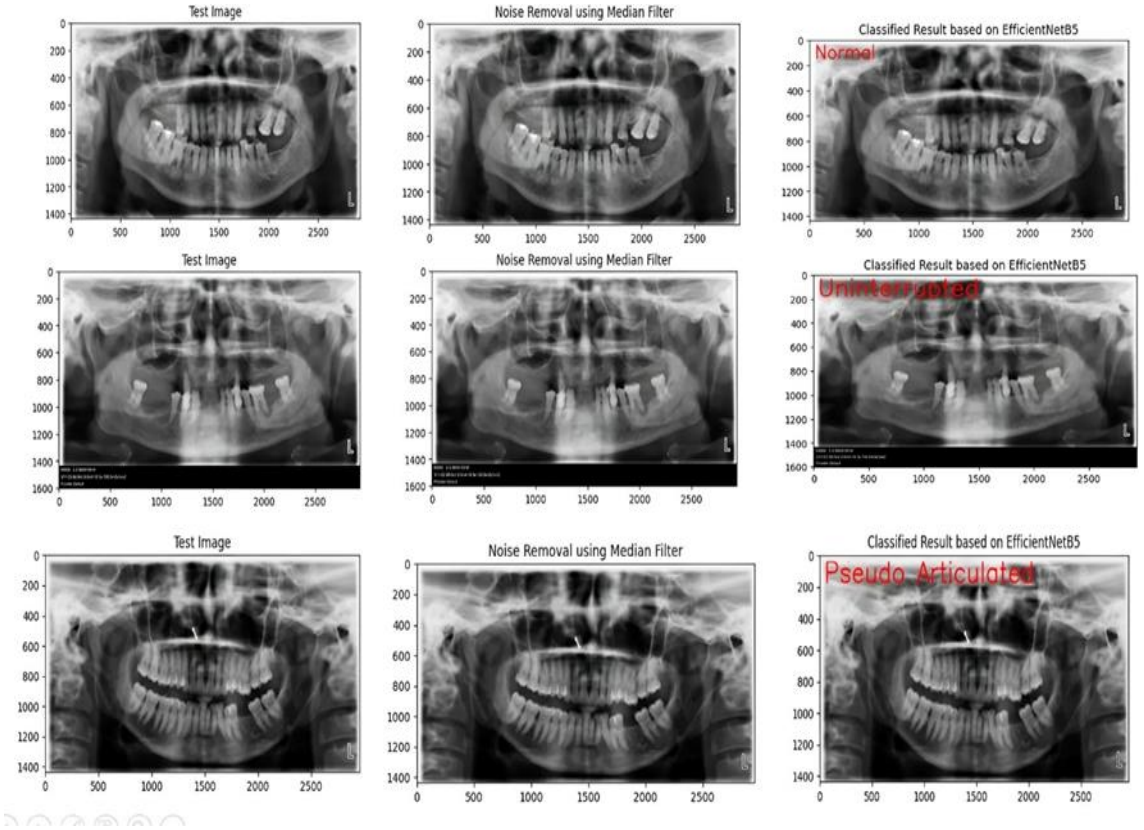

Figure 7. The efficient NetB5 model correctly classifies the lesion.

Performance measure

Confusion matrix

A confusion matrix was constructed to depict the classification behavior of the trained EfficientNetB5 and Inception V3 models when splitting elongated styloid process cases into the four designated categories: "Normal", "Pseudo Articulated", "Segmented", and "Uninterrupted". Every entry in the matrix records how many times the model assigned a specific pairing of actual and predicted classes **(Figure 8)**.

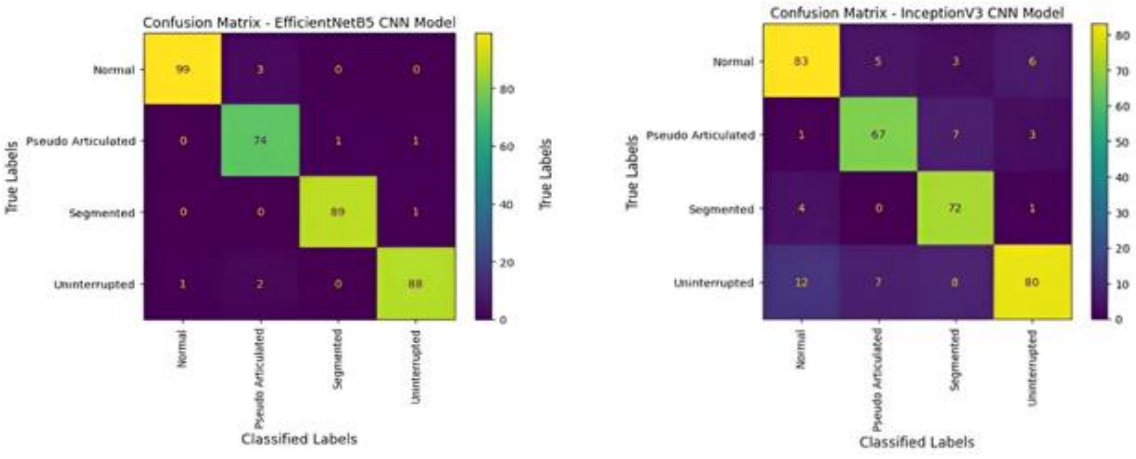

a) b)

Figure 8. Confusion matrix of each model in predicting: "Normal", "Pseudo Articulated", "Segmented", and "Uninterrupted" using the photographs in the test dataset: (a) EfficientNetB5, and (b) Inception V3.

Performance metrics—accuracy, precision, recall, and F1-score

The EfficientNetB5 network recorded an accuracy score of 97.49% and a precision of 98.00%. A recall of 97.00% and an F1-score of 97.00% were also produced, values that jointly summarise the model's holistic performance **(Figure 9)**. For the InceptionV3 counterpart, the accuracy was 84.11%, and the

precision was 85.00%. The same network further posted a recall of 84.00% paired with an F1-score of 84.00% **(Figure 10)**.

Accuracy of the EfficientNetB5 Model: 97.49%

	precision	recall	f1-score	support
0	0.97	0.99	0.98	100
1	0.97	0.94	0.95	79
2	0.99	0.99	0.99	90
3	0.97	0.98	0.97	90
accuracy			0.97	359
macro avg	0.98	0.97	0.97	359
weighted avg	0.97	0.97	0.97	359

Figure 9. Performance metric for the EfficientNetB5 model.

Accuracy of the InceptionV3 Model: 84.11999999999999%

	precision	recall	f1-score	support
0	0.86	0.83	0.84	100
1	0.86	0.85	0.85	79
2	0.94	0.80	0.86	90
3	0.75	0.89	0.81	90
accuracy			0.84	359
macro avg	0.85	0.84	0.84	359
weighted avg	0.85	0.84	0.84	359

Figure 10. Performance metric for the InceptionV3 model.

Figure 11 depicts the ROC plots and corresponding AUC values for both frameworks. EfficientNetB5 achieved an AUC of 0.9825, while Inception V3 achieved 0.8943.

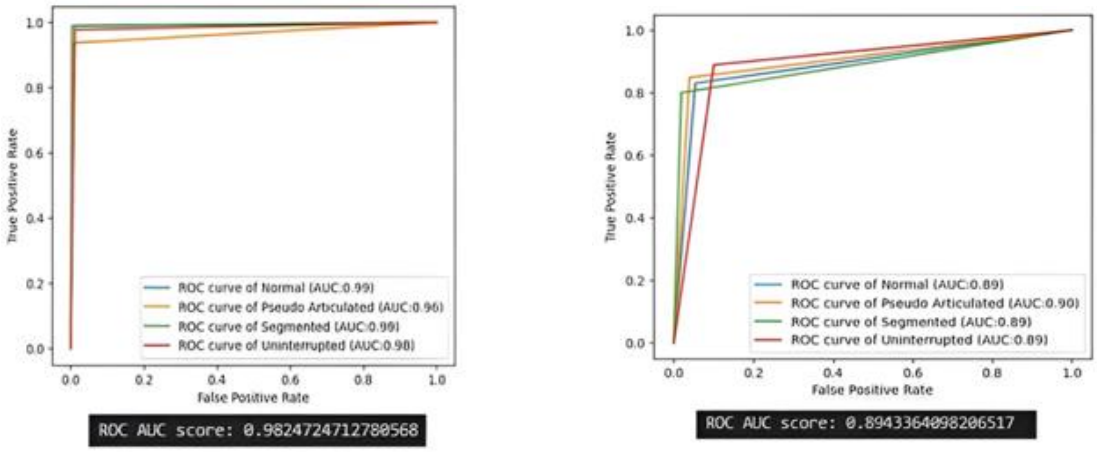

a) b)

Figure 11. ROC curve and AUC analysis: (a) EfficientNetB5, and (b) Inception V3 models.

The temporal bone's styloid process furnishes an anchorage site for a collection of soft-tissue structures: the stylopharyngeus, stylohyoid, and styloglossus muscles, plus the stylomandibular and stylohyoid ligaments. An anatomic elongation of this process—termed elongated styloid process (ESP)—represents a commonplace variant and may precipitate Eagle's syndrome. Symptomatic presentations can encompass dull aching in the pharyngeal region, otalgia, globus sensation in the throat, and dysphagia. On occasion, a mass detectable by palpation inside the tonsillar fossa heightens the discomfort. Because of the close spatial relationships with adjacent structures, establishing the diagnosis is not straightforward; it hinges on meticulous history-taking, physical examination, and imaging to distinguish the entity from confusable conditions such as neuralgias and temporomandibular joint disorders [15]. Effective clinical decision-making—covering both diagnostic classification and therapeutic planning—depends on the correct morphological categorization of elongated styloid processes. In recent years, there has been a marked increase in the adoption of sophisticated computational techniques, most notably deep learning architectures such as CNNs, to automate the classification of medical imagery [16]. AI-enabled evaluation technology yields substantive gains in diagnosing ESP by delivering repeatable, precise measurements of both styloid length and geometry. Relying on such accuracy reduces subjectivity and the potential inaccuracies that plague manual readings, a particularly worthwhile advantage in resource-limited clinical environments. AI-based tools also facilitate the identification of understated irregularities, thereby enabling the prompt detection of associated degenerative pathologies. These deep learning models are adept at isolating critical image features, which empowers them to distinguish elaborate morphological motifs with high fidelity. Tapping into such capabilities holds considerable promise for engineering faster, more dependable ESP classification pipelines. Considered in its entirety, AI-assisted interpretation bolsters diagnostic confidence, simplifies clinical reasoning, and enhances the quality of treatment plans—a benefit most pronounced in operative cases, where an intricate grasp of regional anatomy is imperative.

Deep learning, under the broader umbrella of machine learning, focuses on training artificial neural networks to perform complex tasks by mimicking how the human brain processes incoming information. Its particular potency comes from the capacity to spontaneously detect structure and extract descriptive features straight from data, endowing machines with the faculties to predict, decide, classify, and even anticipate how a patient might respond to therapy. The approach has drawn substantial acclaim and delivered breakthroughs across many sectors, with diagnostic medicine accounting for the lion's share of applications. The work reported here set out to put together a sturdy, deep learning-anchored classification system that could reliably discriminate among distinct ESP subtypes based on digital panoramic radiographs. To that end, the relative capabilities of two non-identical deep learning models—namely, EfficientNetB5 and InceptionV3—were tested on the ESP classification task, with accuracy, precision, recall, and F1 scores measured. Both architectures have previously been trialed across a range of clinical diagnostic undertakings [17-19]. To the best of our knowledge, the present study marks the inaugural exploration of whether artificial intelligence can serve as a trustworthy means for pinpointing and classifying elongation of the styloid process.

During training, these models identify distinctive patterns in images, encoding the characteristic features of elongated styloid processes. These measured values are customarily charted over epochs, which correspond to the number of complete cycles through the whole training dataset. The training accuracy curve depicts how proficiently the model is mastering the correct categorization of the training data, whilst the training loss curve reveals the trajectory of the loss function, which computes the deviation between forecasted and ground-truth values. In the training accuracy graph, a gradual increase in accuracy is expected as epochs progress, indicating that the model is improving its ability to generate precise predictions on the training data. In contrast, within the training loss graph, the objective is to witness a downward trajectory over epochs. A diminishing loss indicates that the model is narrowing the gap between its estimates and the actual figures, thereby boosting its performance. In the context of our work, EfficientNetB5 achieved better model performance than Inception V3.

The EfficientNetB5 architecture yielded an accuracy of 97.49%, whereas InceptionV3 delivered 84.11%, reflecting the proportion of correctly classified instances across all classes. Precision figures of 98.00% for EfficientNetB5 and 85.00% for InceptionV3 highlight the architectures' ability to reliably pinpoint positive instances within each class while minimizing false positives. In addition, the architectures exhibited noteworthy recall of 97.00% in EfficientNet V5 and 84.00% in InceptionV3, underscoring their competence at detecting and recording positive occurrences across the dataset. The

F1-Scores of 97.00% for EfficientNetB5 and 84.00% for InceptionV3 are single metrics that combine precision and recall. It provides a balanced appraisal of model efficacy by accounting for both false positives and false negatives. Altogether, these measurements substantiate the robustness and operational efficiency of the classification framework in correctly diagnosing various categories of elongated styloid processes, thereby illustrating its potential clinical benefit in improving patient treatment outcomes. Parallel investigations using EfficientNetB5 and InceptionV3 architectures were previously undertaken to categorize various pathologies, and both architectures have shown favorable results [17, 20].

The receiver operating characteristic (ROC) curve, alongside the area under the curve (AUC) analysis, provides additional insight into the classification model's ability to separate the four categories of elongated styloid processes. The ROC curve provides a graphical depiction of the trade-off between true positive rate (sensitivity) and false positive rate (1-specificity) across a range of thresholds. An AUC of 0.9825 was observed for EfficientNetB5 and 0.8943 for Inception V3, indicating the model's comprehensive discriminatory power across all categories, with higher values indicating more robust performance. This assessment highlights the model's proficiency in precisely categorizing elongated styloid processes and its potential clinical relevance for supporting clinicians in diagnosing and managing patients with these conditions.

A comparable contemporary study aimed to assess the accuracy of artificial intelligence in detecting elongation of the styloid process on digital panoramic radiographs. It also sought to compare the efficacy of three AI methodologies—logistic regression, neural networks, and Naïve Bayes—within the Orange platform against manual radiographic scrutiny by radiologists. A total of 400 digital panoramic radiographs (OPGs) were examined, and three separate AI frameworks were used to identify elongation of the styloid process. Assessment of performance covered accuracy, sensitivity, specificity, precision, recall, F1 score, and AUC-ROC. Outcomes indicated that logistic regression, together with neural network methodologies, achieved 100% accuracy, with no false positives or false negatives, notching 1.000 across all metrics. The Naïve Bayes framework, though less precise, achieved an AUC of 78%, exceeding chance-level classification, despite 49 false positives and 59 false negatives. Consequently, the investigation concluded that logistic regression and neural network methodologies reliably identified styloid process elongation compared with manual radiographic assessment. Although the Naïve Bayes methodology proved less precise, it nevertheless surpassed chance-level guessing [21].

The current body of work puts forward a deep learning-driven strategy for mechanizing the categorization of elongated styloid processes through the use of digital panoramic radiographs. Harnessing the cutting-edge deep learning designs EfficientNetB5 and InceptionV3, we have substantiated their utility for reliably sorting elongated styloid processes into discrete typologies grounded in their morphological attributes. Our empirical data show that the EfficientNetB5 design achieved a notable accuracy of 97.49%, surpassing that of the InceptionV3 design (84.11%). This outcome indicates that EfficientNetB5 has a stronger ability to classify elongated styloid processes precisely. The elevated accuracy achieved by each design confirms the promise of deep learning methodologies for boosting the efficiency and precision of medical image interpretation workloads. By mechanizing the classification pipeline, our introduced framework offers multiple benefits over conventional manual practices, including reduced reliance on subjective judgment and greater consistency in diagnostic conclusions. Our observations imply that embedding deep learning architectures, particularly EfficientNetB5, into routine clinical workflows could meaningfully improve diagnostic precision and rationalize patient care procedures.

Conclusion

Our investigation fruitfully engineered and substantiated a mechanized framework for identifying and categorizing elongated styloid processes by applying deep learning architectures to digital orthopantomograms. This AI-fueled methodology demonstrated substantial diagnostic precision, with notable potential to reliably detect and classify elongated styloid processes across radiographic images. Said technology represents a notable advancement in mechanizing diagnostic pipelines, delivering more reliable and streamlined results. Moving forward, significant opportunities exist to deploy this technology in real-world clinical environments, where it can bolster diagnostic efficiency and uniformity across diverse patient scenarios, thereby ultimately raising the standard of patient care.

Acknowledgments: We want to thank the Center of Medical and Bioallied Health Sciences and Research at Ajman University, Ajman, UAE.

Conflict of Interest: None

Financial Support: None

Ethics Statement: None

References

1. Assiri Ahmed H, Estrugo-Devesa A, Roselló Llabrés X, Egido-Moreno S, López-López J. The prevalence of elongated styloid process in the population of Barcelona: a cross-sectional study & review of literature. BMC Oral Health. 2023;23(1):674. doi:10.1186/s12903-023-03405-0
2. Kursoglu P, Unalan F, Erdem T. Radiological evaluation of the styloid process in young adults resident in Turkey's Yeditepe University faculty of dentistry. Oral Surg Oral Med Oral Pathol Oral Radiol Endod. 2005;100:491-4. doi:10.1016/j.tripleo.2005.05.061
3. Saccomanno S, Greco F, Corso EDE, Lucidi D, Deli R, D'Addona A, et al. Eagle's syndrome, from clinical presentation to diagnosis and surgical treatment: a case report. Acta Otorhinolaryngol Ital. 2018;38(2):166-9. doi:10.14639/0392-100X-1479
4. Gokce C, Sisman Y, Sipahioglu M. Styloid process elongation or eagle's syndrome: is there any role for ectopic calcification? Eur J Dent. 2008;2(3):224-8. doi:10.1055/s-0039-1697384
5. Ilgüy M, Ilgüy D, Güler N, Bayirli G. Incidence of the type and calcification patterns in patients with elongated styloid process. J Int Med Res. 2005;33:96-102. doi:10.1177/147323000503300110
6. Chen G, Yeh PC, Huang SL. An evaluation of the prevalence of elongated styloid process in Taiwanese population using digital panoramic radiographs. J Dent Sci. 2022;17(2):744-9. doi:10.1016/j.jds.2021.09.033
7. Roopashri G, Vaishali MR, David MP, Baig M. Evaluation of elongated styloid process on digital panoramic radiographs. J Contemp Dent Pract. 2012;13(5):618-22. doi:10.5005/jp-journals-10024-1197
8. Oztunç H, Evlice B, Tatli U, Evlice A. Cone-beam computed tomographic evaluation of styloid process: a retrospective study of 208 patients with orofacial pain. Head Face Med. 2014;10:5. doi:10.1186/1746-160X-10-5
9. Donmez M, Okumus O, Pekiner FN. Cone beam computed tomographic evaluation of styloid process: a retrospective study of 1000 patients. Eur J Dent. 2017;11(2):210-5. doi:10.4103/ejd.ejd_56_17
10. Langlais RP, Miles DA, Van Dis ML. Elongated and mineralized stylohyoid ligament complex: a proposed classification and report of a case of Eagle's syndrome. Oral Surg Oral Med Oral Pathol. 1986;61:527-32. doi:10.1016/0030-4220(86)90400-7
11. Najjar R. Redefining radiology: a review of artificial intelligence integration in medical imaging. Diagnostics. 2023;13(17):2760. doi:10.3390/diagnostics13172760
12. Katsumata A. Deep learning and artificial intelligence in dental diagnostic imaging. Jpn Dent Sci Rev. 2023;59:329-33. doi:10.1016/j.jdsr.2023.09.004
13. Cejudo JE, Chaurasia A, Feldberg B, Krois J, Schwendicke F. Classification of dental radiographs using deep learning. J Clin Med. 2021;10(7):1496. doi:10.3390/jcm10071496
14. Almalki YE, Din AI, Ramzan M, Irfan M, Aamir KM, Almalki A, et al. Deep learning models for classification of dental diseases using orthopantomography x-ray OPG images. Sensors. 2022;22(19):7370. doi:10.3390/s22197370
15. Al-Abrar Ahmad Kailani AA, Sobani MA, Mat Barhan NS, Rahim NA, Mansor M, Lazim NM. Bilateral eagle syndrome: a rare entity. Proc Singap Healthc. 2023;32:20101058231172233. doi:10.1177/20101058231172233
16. Hosny A, Parmar C, Quackenbush J, Schwartz LH, Aerts HJWL. Artificial intelligence in radiology. Nat Rev Cancer. 2018;18(8):500-10. doi:10.1038/s41568-018-0016-5
17. Alshoraihy A, Ibrahim A, Issa HH. Leukemia classification using EfficientNetB5: a deep learning approach. In: 2024 IEEE International Conference on Electronics (ElCon). IEEE; 2024. doi:10.1109/ElCon61730.2024.10468284
18. Srinivas K, Gagana Sri R, Pravallika K, Nishitha K, Polamuri SR. COVID-19 prediction based on hybrid inception V3 with VGG16 using chest x-ray images. Multimed Tools Appl. 2023:1-18. doi:10.1007/s11042-023-15903-y
19. Pan Y, Liu J, Cai Y, Yang X, Zhang Z, Long H, et al. Fundus image classification using Inception V3 and ResNet-50 for the early diagnostics of fundus

diseases. Front Physiol. 2023;14:1126780. doi:10.3389/fphys.2023.1126780

20. Pandiar D, Choudhari S, Poothakulath Krishnan R. Application of InceptionV3, SqueezeNet, and VGG16 convoluted neural networks in the image classification of oral squamous cell carcinoma: a cross-sectional study. Cureus. 2023;15(11):e49108. doi:10.7759/cureus.49108
21. Jeevitha SJ, Kumar SL, Yadalam P. Artificial intelligence: a reliable tool to detect the elongation of the styloid process. Cureus. 2023;15(11):e49541. doi:10.7759/cureus.4954